Accepted manuscript doi:
10.1680/jgeot.22.00010

Submitted: 10 January 2022

Published online in 'accepted manuscript' format: 23 June 2022

Manuscript title: Load history idealization effects for design of monopiles in clay

Authors: Haoyuan Liu*, Nallathamby Sivasithamparam*, Yusuke Suzuki* and Hans Petter Jostad*

Affiliation: *Norwegian Geotechnical Institute (NGI), Oslo, Norway

Corresponding author: Haoyuan Liu, Norwegian Geotechnical Institute (NGI), Oslo, Norway.

E-mail: haoyuan.liu@ngi.no

Accepted manuscript doi:
10.1680/jgeot.22.00010

Abstract

Evaluation of the characteristic behaviour of clay under cyclic loading is desirable and essential for an optimised monopile design of offshore wind turbines (OWT). In current design practice, the irregular storm history is transformed into an idealised regular cyclic history with loading packages of uniform amplitude in ascending order. This paper investigates the effects of load representations by performing a series of load-controlled cyclic triaxial tests. Load histories investigated consist of a calculated one-hour storm loading on an OWT monopile foundation in the North Sea and its representations with different orders of the idealised load packages. The role of the average shear stress is discussed by comparing the shear strain evolution, pore water pressure accumulation, soil stiffness and strength. Cyclic degradation obtained with and without average shear stress components are studied. The experimental investigations in this paper indicate that the current design practice of the load idealisation may not necessarily be conservative. The average shear stress affects the strain accumulation significantly but has relatively minor effects on the pore water pressure evolution. Soil element response subjected to irregular load history is suggested to be investigated more from both experimental and numerical perspectives to develop improved procedure for monopile design.

Keywords: clay; irregular loading; loading idealisation; pore pressures; strain accumulation

Accepted manuscript doi:
10.1680/jgeot.22.00010

INTRODUCTION

Offshore wind energy development is experiencing rapid growth to meet the long-term goal of reducing greenhouse gas emission worldwide. The recent plans for offshore wind farms have a clear tendency of growing in size of turbines at deeper water depth. This tendency naturally results in significant growth in fabrication and installation costs of offshore wind turbines (OWTs), and thus highlights the demands on optimised OWTs foundation design. To achieve cost-effective OWTs design, the governing soil behaviour to the foundation response needs deeper understanding and appropriate consideration.

At present, monopiles dominate the OWTs foundation type. The limit state design methods of monopiles including the Ultimate Limit State (ULS), Fatigue Limit State (FLS) and Serviceability Limit State (SLS) checks (DNV, 2016). The accumulated stain and pore-water pressure in the soil due to environmental loads are relevant to all design criteria (Achmus *et al*., 2009; Houlsby, 2016; Jostad *et al*., 2020).

Both experimental and numerical approaches are in recent years used to investigate the tilting of monopiles when subjected to cyclic loads (LeBlanc *et al*., 2010; Cuéllar *et al*., 2014; Houlsby *et al*., 2017; Liu *et al*., 2021). Within the scope of the three-dimensional finite element analysis (3D FE) approach, two categories of analyses can be distinguished according to the constitutive models adopted – i.e., implicit models (constitutive models that follows the entire stress-strain response for the actual time history, as adopted for instance in Liu & Kaynia (2021)) and explicit models (constitutive models that calculate the accumulated and cyclic strain as a function of the number of regular load cycles, for instance, Niemunis *et al*. (2005) and Jostad *et al*. (2014)). When performing explicit 3D FE, the environmental loading, despite of the irregular and multi-directional features in nature, is usually translated into idealised regular cyclic loading packages (uniform cyclic loading amplitude within a package, with the packages arranged in ascending order in cyclic amplitude (Andersen, 2015)). The accumulated displacement and rotation of a monopile are calculated through the concept of 'equivalent number of cycles' - with the effect of previous stress cycles and non-linearity of soil behaviour being considered (Andersen *et al*., 1992). The underlying assumption in the calculation of the accumulated displacement and rotation is that the effect of cyclic loading can be defined by a state parameter that is independent of the actual history as accumulated pore pressure, accumulated strain or cyclic degradation of stiffness. However, extensive discussions are still going on regarding the loading package ordering effect (Wichtmann *et al*., 2010; Norén- Cosgriff *et al*., 2015; Liu *et al*., 2022).

One recent study on this aspect from soil element performance perspective comes from Zografou *et al*. (2019). Cyclic direct simple shear (DSS) tests were performed on normally consolidated Kaolin clay. The load histories are idealised representations of an irregular environmental load (i.e., average load level and load amplitude of the cyclic load history keep varying with time, in what follows referred as 'irregular loading') but with different arrangement of the loading packages. One of the observation is that, organising the idealised loading packages in ascending-amplitude order gives larger total strain than obtained from idealised loading histories with loading packages in other orders. Such a conclusion supports the current design practise.In the work, however, no experimental soil tests on a truly irregular load history was conducted.

Skau *et al*. (2022) performed undrained cyclic DSS tests on a lightly over-consolidated clay under irregular loading and various idealised regular loading histories. The experimental results showed that, for load histories with significant averageload, the soil accumulated less permanent strain when subjected to a conventional idealised load history – comparing to the situation where the actual irregular load history was applied. This raises awareness of critical

evaluation regarding the applicability of transformation of irregular loading to idealised representation.

This paper supplements the works mentioned above by providing experimental evidence but focuses on both stress-strain behaviour and pore water pressure evolution under cyclic triaxial stress paths. The test results at soil element level are expected to shed light on the prediction of full-scale monopile foundation rotation and lateral displacements. The work particularly investigates on: (1) the effect of load-history idealisation commonly adopted in design practice; (2) the effects of ordering of idealised loading packages; (3) the role of the average shear stress component on the clay's cyclic and accumulated shear strains and (4) pore water pressure accumulation under different loading histories.

For this purpose, a series of undrained cyclic triaxial tests were performed on normally consolidated reconstituted clay specimens subjected to an irregular storm loading and its four different load representations. The aim of the paper is to investigate the difference of clay cyclic behaviour caused by the applied load pattern: the effects of soil reconstitution and disturbance are not investigated under the primes of similar cyclic behaviour for intact soils and reconstituted soils at qualitative level (Andersen *et al*., 1992). For a real design case, the effects of soil sampling should be considered quantitatively (Fearon & Coop, 2000; Long *et al*., 2010; Chu *et al*., 2017; Taukoor *et al*., 2019).

EXPERIMENTAL APPROACH AND PROGRAMS

Test apparatus

A series of cyclic triaxial tests were performed using the advanced dynamic triaxial testing system (DYNTTS) developed by GDS Instruments and adapted at the NGI Oslo laboratory. The system has a dynamic electromechanical actuator capable of applying load at up to 5 Hz. It has been modified to take into account false deformation due to the cell expansion. The system allows users to define unique wave-forms as input cyclic loading motion, in addition to sinusoidal wave-forms typically used for cyclic testing. The detailed information of the test system is given by Suzuki *et al*. (2017). In this testing program, the cyclic tests were performed by load-control and target load sequences were prepared in stages for irregular cyclic loading or sinusoidalcyclic loading packages.

Test material

Identical slurry-based reconstituted Onsøy clay specimens were used in this testing program. A batch of Onsøy clay was originally sampled about 15 years ago, from shallow depths of 1 to 2m in the Onsøy area in Norway, referred as Onsøy historic sites (Gundersen *et al*., 2019). The clay was fully remoulded and mixed into a slurry state at a water content of 120% and then one-dimensionally pre-consolidated up to a vertical stress of 50 kPa with several loading stages over four weeks in a large box. The clay samples were cut, stored and used for the triaxial tests. The initial dimensions of the triaxial specimens were nominally a height of 110 mm and a diameter of 54 mm. The initial water contents of the specimens were between 58% and 61% . The tested material has index properties of plastic limit of 29% , liquid limit of 68% and plasticity index of 39. The ratio of undrained shear strength to effective vertical stress at the normally consolidated condition $(s_{uC} / \sigma_{a0}')_{NC}$ of about 0.286 of the tests material (Suzuki *et al*., 2017). Details of the tested clay characterization and engineering properties from the recent research are summarised in Long & Donohue (2010) and Yang *et al*. (2020).

Accepted manuscript doi:
10.1680/jgeot.22.00010

Test procedure

A consistent test procedure was used for all the tests: flushing of filters and lines at a confining pressure of $10kPa$, applying a back-pressure of $1000kPa$, increasing both the axial and radial effective stresses by ramping at $20kPa/h$, followed by ramping the axial effective stress at $2kPa/h$ for the anisotropically consolidated tests (see Table 1). Skepmton's B-value was checked prior to the cyclic stage and a minimum value of 0.95 was achieved. Bender element measurements were also carried out prior to the cyclic stage. The small strain shear modulus measured by the bender elements and water content after consolidation are summarised in Table 1. Cyclic loading stages were then executed, as described in the following section.

Notation

The shear stress and strain components are defined as illustrated in Fig. 1. Initial effective average normal stress s'_0 is defined as $s'_0 = \left(\sigma'_{a0} + \sigma'_{r0}\right)/2$, where σ'_{a0} and σ'_{r0} stand for the effective axial and radial stresses prior to the shearing in triaxial tests. The shear stress τ is defined as $\tau = \left(\sigma'_a - \sigma'_r\right)/2$, where σ'_a and σ'_r stand for the current effective axial and radial stresses,respectively. For regular load history, average shear stress $\tau_{av} = \left(\tau_{peak} + \tau_{trough}\right)/2$, where τ_{peak} and τ_{trough} are the maximum and minimum shear stress of the constant-amplitude loading program, respectively. The average shear stress can also be computed as the sum of the shear stress at the end of consolidation τ_0 and the average component of the applied shear load history $\Delta\tau_a$. Cyclic shear stress $\tau_{cy} = \left(\tau_{peak} - \tau_{trough}\right)/2$. Shear strain γ is defined as $\gamma = \varepsilon_a - \varepsilon_r$, where ε_a is the axial strain and ε_r is the radial strain in a triaxial test. The average shear strain $\gamma_{av} = \left(\gamma_{peak} + \gamma_{trough}\right)/2$, where γ_{peak} represents the shear strain corresponding to the shear strain level at $\tau = \tau_{peak}$ and γ_{trough} represents the shear strain corresponding to the shear strain level at $\tau = \tau_{trough}$. Cyclic shear strain $\gamma_{cy} = \left(\gamma_{peak} - \gamma_{trough}\right)/2$.

Test program

The considered load case for the laboratory test program is based on a time domain analysis of an offshore wind turbine in North Sea and reflects a ULS load situation, with wind speed and sea state conditions of a 50 years return period for a North Sea site in 30m water depth (Li *et al*., 2013). The load was extracted from a global time domain analysis of the OWT system include wind, waves and rotor dynamics. The storm loading history has a duration of 36-hour with a wind speed of 38.5m/s, significant wave height (H_s) of 9.5m and a spectral peak period T_p of 12.3s. The situation reflects DLC (Design Load Case) 6.1 without considering any yaw misalignment (IEC, 2019). The dominating cyclic load frequency of the history is about 0.25 Hz (i.e.,cyclic loading period of 4s). The selected 1-hour load history contains no significant average environmental load.

Accepted manuscript doi:
10.1680/jgeot.22.00010

Five test histories are designed based on the storm loading history by applying constant ratio between recorded load and applied shear stresses in the soil. The test histories are summarised in Table 1 and introduced below:

- **IRL_A20**: Irregular loading history which is re-scaled based on a 1-hour peak-loading period in the recorded 36-hour loading history (as illustrated in Fig. 2a), with average shear stress $\tau_{av} = 20$ kPa due to $K_0 = 0.6$ and $\sigma'_{v0} = 100kPa$.
- **IDL_A20**: Idealised regular loading history of **IRL_A20**. In design practice, the irregular loading history is conventionally converted into an idealised regular loading history that includes loading packages of constant cyclic loading amplitude (within each loading package). The loading packages are organised in ascending amplitude order, as presented in Fig. 2b. In this work, the modified rainflow counting method (Norén-Cosgriff *et al*., 2015) is used to count the occurrence of the different amplitudes. The arrangement of the loading packages is summarized in Table 2. The average shear stress $\tau_{av} = 20$ kPa ($K_0 = 0.6$) and $\sigma'_{v0} = 100kPa$.
- **MS_A20**: Mix-sorted idealised loading history (Fig. 2c). Loading history **MS_A20** has the same number of cycles as **IDL_A20**. Loading packages are arranged so that **MS_A20** can correspondingly reflect the first intensive shearing period and the occurrence of the largest load amplitude level of **IRL_A20** – both happened during the first 5 minutes (see the loading range in dash-line boxes in Fig. 2a and 2c). The arrangement of the load parcels in the rest of the load history is arbitrary but aims to have relatively large load cycles spanning across the 55 minutes duration. The load parcels are summarized in Table 3. The average shear stress $\tau_{av} = 20$ kPa (due to $K_0 = 0.6$ and $\sigma'_{v0} = 100kPa$).
- **IDL_A0**: Idealised regular loading history with the average shear stress $\tau_{av} = 0$ ($K_0 = 1$, Fig. 2d). The arrangement of loading packages is summarized in Table 2.
- **MS_A0**: Mix-sorted loading history with the average shear stress $\tau_{av} = 0$ ($K_0 = 1$, Fig. 2e). The arrangement of loading packages is summarized in Table 3.

No significant average environmental load component appears in the recorded storm load, the scaled stress thus should have $\Delta\tau_a = 0$. Given that $\sigma'_{a0} = 100kPa$ and $K_0 = 0.6$, $\tau_0 = (1-0.6)100/2 = 20kPa$, $\tau_{av} = \tau_0 + \Delta\tau_a = 20kPa$. Following the assumption of $\tau_{cy}^{max} / \tau_{av} = 1$, $\tau_{cy}^{max} \approx 20kPa$ (the applied $\tau_{cy}^{max} = 21.4kPa$ as indicated in Table 1).

Load cases **IDL_A0** and **MS_A0** are designed to study the role of average shear stress on shear strain variation by comparing the simulation results of **IDL_A20** and **MS_A20**.

The soil samples of tests **IDL_A0** and **MS_A0** are prepared under the condition of effective overburden stress equals to $50kPa$ prior to the consolidation stage. To eliminate the overburden stress effects and reach normally consolidated state, the clay samples of tests **IDL_A0** and **MS_A0** are consolidated isotropically up to $\sigma'_{a0} = \sigma'_{r0} = 150$ kPa.

To obtain comparable results with test histories **IRL_A20**, **IDL_A20** and **MS_A20**, the cyclic amplitudes for tests **IDL_A0** and **MS_A0** are calculated as $150/\left[(100+0.6*100)/2\right] = 1.875$ times the corresponding cyclicamplitudes in tests **IDL_A20** and **MS_A20**. In this way, the corresponding initial cyclic amplitude ratio (defined

as $\tau_{cy} / s_0^{'}$) for each loading parcel is the same for tests **IDL_A20** and **IDL_A0** (**MS_A20**and **MS_A0**).

Though the σ'_{a0} level in tests **IDL_A0** and **MS_A0** is higher than that in tests **IRL_A20**, **IDL_A20** and **MS_A20**, the effects of the different consolidation stresses are assumed to be eliminated since the conclusions in this paper are derived by normalising the shear stresses by the selected consolidation stresses.

Identical additional cycles, referred to as reference cycles, are applied at the end of each loading history (until soil failure) to investigate the influence of different representations of storm loading history on soil degradation. Reference cycles are selected to have the same amplitude as the largest amplitude group in the idealised histories (see Tables 2 and 3).

EXPERIMENTAL RESULTS

The experimental tests are divided into two sets based on the level of average shear stress (i.e., $\tau_{ave} = 20kPa$ and 0 .) Reliable comparisons can be achieved only if the tested samples are comparable under the condition of the same initial stress sate for each set. For this purpose, the small strain stiffness G_{max} of each sample is presented in Table 1. The G_{max} values measured after consolidation prior to cyclic loading are almost identical and comparable among each consolidation stress condition. However, the magnitude of G_{max} has no direct influence on the discussion in this work.

Loading history effects on strain accumulation

The experimental results of all 5 tests are presented in Fig. 3, in terms of normalised stress path ($\tau / \sigma'_{a0} \sim \sigma'_v / \sigma'_{a0}$), normalised stress-strain response ($\tau / \sigma'_{a0} \sim \gamma$) and the normalised stress-pore water pressure ratio ($\tau / \sigma'_{a0} \sim u_p / \sigma'_{a0}$). The evolution of the color indicate the time change as indicated by color bars.

For irregular load case **IRL_A20** and mix sorted load cases **MS_A20** and **MS_A0**, obvious reduction of the effective vertical stress is observed at the early stage of the loading (for example, within the first 10 minutes) – the phenomenon is different from those of idealised regular load cases **IDL_A20** and **IDL_A0** where apparent reduction of effective vertical stress can only be found at the last 10 minutes of the loading (corresponding to the cyclic stress amplitude ratio of greater than 0.55). The obvious reduction of the effective vertical stress in load cases **IRL_A20**, **MS_A20** and **MS_A0** are the direct consequence of the accumulation of the excess pore water pressure. From Fig. 3, rapid pore water pressure increase can be observed each time there is load cycle with significant shear stress ratio being applied. Same trend applies to the shear strain evolution. For load cases with $\tau_{av} = 0$, there isalmost no accumulated strain.

Fig. 3 shows the overall similarities and differences regarding the soil response among different load cases. Detailed study will be presented in the following sections on aspects of strain accumulation and pore water pressure accumulation, respectively. The role of average shear component is also discussed.

Strain accumulation

Effect of ordering of loading cycles on sand cyclic behaviour has been studied from experimental point of view regarding both pore water pressure accumulation (Tatsuoka *et al.*, 1986) and strain accumulation (Stewart, 1986; Wichtmann *et al.*, 2010). Later on, numerical approach has also been adopted to study the load history effects on the strain accumulation of

soil and monopile tilting (Liu *et al*., 2022) – targeting for sand material under drained condition.

In this work, effects of the sequence of load cycles are checked against laboratory tests results on clay, for irregular loading history (**IRL_A20**), idealised loading histories (ascending amplitudes **IDL_A20** and mix-sorted **MS_A20**). For this purpose, the strain accumulation results from the three different representations of the load histories are presented in terms of shear strain versus time in Fig. 4 (to make close link between the load historiesand strain accumulation, the stress ratios are also included in the same plot).

The stress levels in Fig. 4 are represented by the stress ratios defined as τ / s', where $s' = \left(\sigma'_a + \sigma'_r\right)/2$ calculated at the end of each loading cycle. The largest accumulated strain is developed by the irregular load history **IRL_A20**, with an accumulated shear strain $\gamma_{acc} = 4.5\%$ at the end of the load history (where γ_{acc} is recorded at the end of a loading cycle when $\tau = \tau_{av}$). The accumulated shear strain is significantly larger than the shear strain (0.25%) triggered by the idealised regular load history with ascending-amplitude load packages (**IDL_A20**). The idealised load history with the mix-sorted packages results in intermediate accumulated shear strain – $\gamma_{acc} = 1.7\%$. Considering theaccumulated strain, the conventional treatment of the irregular loading history in industry design – i.e., transforming the loading history into loading packages with ascending amplitudes brings the design into non-conservative predictions. Such a conclusion disagrees with the conclusion of Zografou *et al*. (2019) where the strain accumulation results of irregular loading case is not considered.

Another observation from Fig. 4 is that the accumulated shear strain increases each time a loading parcel with significant stress ratio – but not necessarily the maximum ever load ratio – is applied (see Fig. 4b). For loading history **IRL_A20**, at $t = 36.4\,\text{min}$, the maximum shear stress ratio is applied the first time (loading package 5 as indicated in Table 3), However, significant increase of γ is still observed in the following loading process, for instance during time interval t=[40.7min, 50.4min] and, less obviously, t=[51min, 59min]. For loading history **MS_A20**, the maximum shear stress ratio is applied at $t = 42.4\,\text{min}$, while accumulated strain still increases obviously between t=[42.4min, 43.6min].

Behaviour of reference cycles

Fig. 5 shows the shear strain versus the number of references cycles applied after the load histories **IRL_A20**, **IDL_A20** and **MS_A20**. The figure shows that the test with the irregular load history **IRL_A20** requires two cycles to accumulate 15% shear strain; the idealised load history with mixed ordering **MS_A20** requires four cycles, while the idealised load history **IDL_A20** with ascending shear amplitude packages require about eight cycles. This demonstrates that the different representations of the load history have different impact on the soil, and the irregular load history degrades the soil the most among the investigated loading histories. This is also seen when the stress-strain loop for the first reference cycles is plotted (see Fig. 6). The current design practice with transformation of the irregular load history into packages of uniform amplitude in ascending order underestimate the accumulated strain in normal consolidated clay significantly.

Fig. 7 compares the average and the cyclic component of the shear strain within the first reference cycles of loading histories **IRL_A20**, **IDL_A20** and **MS_A20**. For loading histories with significant average shear stress, the average strain dominates the strain accumulation – this conclusion agrees with the cyclic DSS test results reported by (Skau *et al*., 2022). For the test result of load history **IDL_A20**, the average andcyclic shear strain (γ_{av} and γ_{cy}) level are similar and small for the first reference load cycle. To make the

Accepted manuscript doi:
10.1680/jgeot.22.00010

comparison clear, γ_{av} and γ_{cy} of the 5^{th} loading cycle are also included in the figure – the average strain dominates the accumulated strain, as expected.

Role of average shear stress on shear strain variation

The average shear stress level τ_{av} is assumed to promote the distinct difference in strain accumulation for loading histories **IRL_A20**, **IDL_A20** and **MS_A20**. To check this assumption, idealised and mix-sorted idealised loading histories **IDL_A20** and **MS_A20** are scaled and applied to the isotopically consolidated clay specimens, i.e., loading cases **IDL_A0** and **MS_A0**, with the average shear stress level $\tau_{av} = 0$. The average strains for loading cases **IDL_20** and **MS_20** are compared with the average strains triggered in load cases **IDL_A20** and **MS_A20** in Fig. 8. For loading histories **IDL_A0** and **MS_A0**, very small (nearly zero) accumulated shear strains γ_{acc} is developed (the non-zero accumulation of strain is believed due to the slight soil anisotropy from sample preparation).

Fig. 9 shows the shear strain versus number of reference cycles applied after the load histories **IDL_A0** and **MS_A0**. To reach 15% shear strain, the idealised load history **IDL_A0** requires five reference loading cycles; while for mix-sorted load history **MS_A0**, nine reference cycles are needed. Under the premise of zero average shear stress, the idealised load history with packages in ascending order degrades the soil more significantly than the mix-sorted load history. The results disagree with the conclusion from Fig. 5 where the load histories have significant average shear stress. Fig. 10 presents the stress-strain loop of the first reference cycle for loading histories **IDL_A0** and **MS_A0**. The secant stiffness of the stress-strain loop of **IDL_A0** is obviously smaller than the secant stiffness obtained from **MS_A0**. This result is also different from the conclusion from Fig. 6 (i.e., results of loading histories with $\tau_{av} = 20\,\text{kPa}$).

Pore pressure accumulation

Accumulation of pore water pressure (together with the irrecoverable strain) affects the stiffness and strength of soil. Proper estimation on pore water pressure accumulation in soil is of great importance for ULS and SLS assessment of OWTs foundations. In this section, the pore water pressure evolution subjected to different loading histories are presented and discussed. The pore water pressure is measured at the two ends of the clay specimen. However, one may realise that the distribution of pore pressure in clay during cyclic loading may not be uniform within the specimens – especially for triaxial size specimen and relatively short loading period ($4s$ for irregular loading in this study). These experimental limitations may affect the direct comparison with other experimental results in quantity level.

Pore pressure accumulation with presence of τ_{av}

Fig. 11 summarises the evolution of pore water pressure for loading histories **IRL_A20**, **IDL_A20** and **MS_A20** (both step-by-step pore water pressure evolution and the corresponding average pore water pressure levels for each test are presented).

the coloured lines represent the step-by-step pore water pressure evolution; the black lines are the corresponding average pore water pressure levels for each test).

Rapid pore water pressure accumulation is observed from $t = 2.7\,\text{min}$ (when the loading parcel with the largest amplitude is applied) for irregular loading case **IRL_A20**. After $t = 2.7\,\text{min}$, the pore water pressure level keeps increasing and reaches 24kPa at the end of the 60 minutes of loading.

For idealised loading history with ascending amplitudes (**IDL_A20**), pore water pressure accumulates for $\tau_{cy} / \tau_{max}^{cy} > 0.8$ (i.e., loading packages 8 and afterwards in Table 2) – no significant pore water pressure being accumulated for loading packages with smaller amplitudes.

Accumulation of pore water pressure for mix-sorted idealised loading case (**MS_A20**) starts from the onset of the test. However, the rapid increase of pore water pressure occurs at t=2.7min when the maximum loading amplitude is applied, same as loading case **IRL_A20**. At t=60min, pore water pressure triggered by loading case **MS_A20** reaches about 28kPa, which is only slightly larger than the results obtained from loading **IRL_A20** (24kPa), all significantly larger than that obtained from idealised loading case **IDL_A20**. This indicates that, for pore water pressure accumulation, it is not conservative to put the loading packages with the largest amplitudes at the end of a representative loading history. This is in line with the conclusion drawn from the strain accumulation pattern.

Pore pressure accumulation with $\tau_{av} = 0$

Fig. 12 compares the accumulated pore water pressure ratio r_u^{acc} evolution against time for loading cases **IDL_A20**, **MS_A20**, **IDL_A0** and **MS_A0**. The accumulated pore water pressure ratio r_u^{acc} is defined as u^{acc} / s_0, where u^{acc} indicates the accumulated pore water pressure (i.e., the pore water pressure at the end of a loading cycle).

As already discussed, for loading history with the presence of τ_{av}, the mix-sorted idealised loading (**MS_A20**) triggers significant ultimate r_u^{acc} compared to the result of idealised loading (**IDL_A20**). The same for cyclic loading history with $\tau_{av} = 0$: the ultimate r_u^{acc} triggered by loading history **MS_A0** (mix-sorted) is higher than that triggered by **IDL_A0** (idealised). Besides, under the premise of the same cyclic stress amplitude ratios, almost the same ultimate r_u^{acc} ratio (0.15 for idealised loading histories **IDL_A20** and **IDL_A0**; 0.3 for mix-sorted idealised loading histories **MS_A20** and **MS_A0**) is achieved for loading histories with the same order of loading packages, independently from the τ_{av} levels. The loading history (i.e., at what time the maximum cyclic loading amplitude is applied) affects the ultimate pore water pressure level. For the same type of loading history, the accumulated pore water pressure in clay is dependent on the cyclic amplitudes but less affected by the presence of average shear stress. However, such a conclusion is derived under the condition that the accumulated pore water pressure is low. In this case, maximum pore water pressure ratio is about 0.3 (see Fig. 3 and Fig. 12).

DISCUSSION

The comparison results in this work indicate that if a high shear stress appears at early stage of an irregular loading, the load idealisation of ascending cyclic amplitude order underestimates the soil degradation. Excess pore water pressure is generatedsignificantly when the maximum applied shear stress ratio is exceeded. For loading cases **IRL_A20** and **MS_A20**, loading cycles with large amplitude occurs at early stage (i.e., within the first 5 minutes, as indicated in Fig. 2), rapid excess pore water pressure generation during this time period (see Figs. 11 and 12). The effective stress reduction is therefore apparent as illustrated in Fig. 3. The subsequent shearing, although may have the same average shear stress, would have higher shear stress ratio (see Fig. 4) and thus leads to larger accumulated pore water pressure and shear strain.

Accepted manuscript doi:
10.1680/jgeot.22.00010

For load cases with an average stress level, the two idealised loading cases (**IDL_A20** and **MS_A20**) result in less soil degradation than that of the irregular load case (**IRL_A20**). Relatively less soil degradation in **IDL_A20** and **MS_A20** can be attribute to the loss of some of the high average or peak loads in the original irregular loading – as indicated in Fig. 13 where the first 5 minutes load histories of **IRL_A20** and tbfMS_A20 are presented: for load case **IRL_A20**, the average shear stress keep varying during the selected time duration. While for load case **MS_A20**, constant average shear stress is used in each load package. Change of the average shear stress component promotes the development of shear strain and in the end results in larger accumulated strain in the irregular load case as also indicated by Fig. 3.

The observations of this work are limited to cyclic contractive behaviour of normal consolidated clays. Cyclic loading idealization effects on strongly dilative clays needs further investigate.

CONCLUSION

In this paper, loading history effects on the cyclic behaviour of a normally consolidated clay are investigated. A one-hour peak-loading period from a time domain analysis of an offshore wind turbine in North Sea is selected as the irregular loading case.Idealised regular loading histories with packages with ascending cyclic amplitude order and idealised regular histories with mix-sorted loading packages are transformed from the irregular loading case.

The accumulated shear strain is dependent on the presence of average shear stress. The irregular loading history generates the largest accumulated shear strain and gives most significant soil degradation among the investigated load cases. The idealised loading history with packages with ascending cyclic shear stress amplitude accumulates least shear strain and the least soil degradation. The conventional treatment in design practise (i.e., transforming the irregular loading history into the history with idealised ascending-amplitude loading packages) underestimates the accumulated strain if there is a significant average shear stress component – proper safety margin should be given when using this approach. In monopile design practice, it is recommended to investigate extensively the soil behaviour subjected to irregular loading both experimentally and numerically in future researches.

For loading histories with average shear stress around 0, applying some large-amplitude load cycles at the early stage of the idealised load history degrades soil more than loading history with packages in ascending-amplitude order. The experimental results regarding strain accumulation indicate that the average shear stress govern the accumulation of shear strain under different loading history conditions.

The loading history also affects the pore water pressure accumulation in normally consolidated clay. Applying loading cycles with large amplitudes at the beginning of a loading history accelerate the generation of pore water pressure. Comparable pore water pressure level is achieved for irregular loading history and idealised mix-sorted loading history, both significantly larger than that developed by the idealised history with ascending cyclic shear stress amplitude. Different from the strain accumulation, it is the cyclic amplitude, and not the average shear stress, that govern the accumulation of pore water pressure in premise of small accumulated pore water pressure ratio.

Acknowledgements

The authors gratefully acknowledge the support from the Wave Loads and Soil Support for Extra-Large Monopiles (WAS-XL) project (NFR grant 268182). In addition, the authors would like to thank colleagues at NGI for valuable discussions, in particular Dr. Knut Andersen.

References

Achmus, M., Kuo, Y.-S. & Abdel-Rahman, K. (2009). Behavior of monopile foundations under cyclic lateral load. *Computers and Geotechnics* 36, No. 5, 725–735.

Andersen, K., Dyvik, R., Kikuchi, Y. & Skomedal, E. (1992). Clay behaviour under irregular cyclic loading. In *Proceedings of the international conference on the behaviours of offshore structures*, vol. 2, p. 937–950.

Andersen, K. H. (2015). Cyclic soil parameters for offshore foundation design. *Frontiers in offshore geotechnics III* 5.

Chu, J., Keng, B., Lee, Y. & Gan, C. (2017). The shear strength and consolidation behaviour of reconstituted singapore marine clay. In *Soft Soil Engineering*, Routledge, pp. 669–674.

Cuéllar, P., Mira, P., Pastor, M., Merodo, J. A. F., Baeßler, M. & Rücker, W. (2014). A numerical model for the transient analysis of offshore foundations under cyclic loading. *Computers and Geotechnics* 59, 75–86.

DNV (2016). DNVGL-ST-0126: Support structures for wind turbines. *Oslo, Norway: DNV GL*.

Fearon, R. & Coop, M. (2000). Reconstitution: what makes an appropriate reference material? *Géotechnique* 50, No. 4, 471–477.

Gundersen, A., Hansen, R., Lunne, T., L Heureux, J.-S. & Strandvik, S. O. (2019). Characterization and engineering properties of the ngts onsøy soft clay site. *AIMS Geosciences* doi: 10.3934/geosci.2019.3.665.

Houlsby, G. (2016). Interactions in offshore foundation design. *Géotechnique* 66, No. 10, 791–825.

Houlsby, G., Abadie, C., Beuckelaers, W. & Byrne, B. (2017). A model for nonlinear hysteretic and ratcheting behaviour. *International Journal of Solids and Structures* 120, 67–80.

IEC (2019). Wind energy generation systems-part 3-1: Design requirements for fixed offshore wind turbines. *International standard IEC* , 61400–3.

Jostad, H., Grimstad, G., Andersen, K., Saue, M., Shin, Y. & You, D. (2014). A FE procedure for foundation design of offshore structures–applied to study a potential owt monopile foundation in the korean western sea. *Geotechnical Engineering Journal of the SEAGS & AGSSEA* 45, No. 4, 63–72.

Jostad, H. P., Dahl, B. M., Page, A., Sivasithamparam, N. & Sturm, H. (2020). Evaluation of soil models for improved design of offshore wind turbine foundations in dense sand. *Géotechnique* , 1–18.

LeBlanc, C., Byrne, B. & Houlsby, G. (2010). Response of stiff piles to random two-way lateral loading. *Géotechnique* 60, No. 9, 715–721.

Li, L., Gao, Z. & Moan, T. (2013). Joint environmental data at five european offshore sites for design of combined wind and wave energy devices. In *International Conference on Offshore Mechanics and Arctic Engineering*, vol. 55423, American Society of Mechanical Engineers, p. V008T09A006.

Liu, H. Y. & Kaynia, A. M. (2021). Characteristics of cyclic undrained model sanisand-msu and their effects on response of monopiles for offshore wind structures. *Géotechnique* , 1–16.

Liu, H. Y., Kementzetzidis, E., Abell, J. A. & Pisanò, F. (2021). From cyclic sand ratcheting to tilt accumulation of offshore monopiles: 3d fe modelling using sanisand-ms. *Géotechnique*, 1–16.

Liu, H. Y., Pisanò, F., Jostad, H. P. & Sivasithamparam, N. (2022). Impact of cyclic strain accumulation on the tilting behaviour of monopiles in sand: An assessment of the miner's rule based on sanisand-ms 3d fe modelling. *Ocean Engineering* 250, 110579.

Long, M. & Donohue, S. (2010). Characterization of norwegian marine clays with combined shear wave velocity and piezocone cone penetration test (cptu) data. *Canadian geotechnical journal* 47, No. 7, 709–718.

Long, M., Gudjonsson, G., Donohue, S. & Hagberg, K. (2010). Engineering characterisation of norwegian glaciomarine silt. *Engineering geology* 110, No. 3-4, 51–65.

Niemunis, A., Wichtmann, T. & Triantafyllidis, T. (2005). A high-cycle accumulation model for sand. *Computers and geotechnics* 32, No. 4, 245–263.

Norén-Cosgriff, K., Jostad, H. & Madshus, C. (2015). Idealized load composition for determination of cyclic undrained degradation of soils. In *Frontiers in Offshore Geotechnics III: Proceedings of the 3rd International Symposium on Frontiers in Offshore Geotechnics (ISFOG 2015)*, vol. 1, Taylor & Francis Books Ltd, pp. 1097–1102.

Skau, K., Dahl, B., Jostad, H., Suzuki, Y., Sordi, J. & Havmøller, O. (2022). Response of lightly over-consolidated clay under irregular cyclic loading and comparison with predictions from the strain accumulation procedure. *Géotechnique* in press.

Stewart, H. E. (1986). Permanent strains from cyclic variable-amplitude loadings. *Journal of Geotechnical Engineering* 112, No. 6, 646–660.

Suzuki, Y., Dyvik, R. & Schmertmann, J. H. (2017). Experimental study on use of internal and external drains in triaxial tests. *Geotechnical Testing Journal* 40, No. 5, 810–821.

Tatsuoka, F., Maeda, S., Ochi, K. & Fujii, S. (1986). Prediction of cyclic undrained strength of sand subjected to irregular loadings. *Soils and Foundations* 26, No. 2, 73–90.

Taukoor, V., Rutherford, C. J. & Olson, S. M. (2019). Cyclic behavior of a reconstituted gulf of mexico clay. In *Geo-Congress 2019: Earthquake Engineering and Soil Dynamics*, American Society of Civil Engineers Reston, VA, pp. 313–321.

Wichtmann, T., Niemunis, A. & Triantafyllidis, T. (2010). Strain accumulation in sand due to drained cyclic loading: on the effect of monotonic and cyclic preloading (miner's rule). *Soil Dynamics and Earthquake Engineering* 30, No. 8, 736–745.

Yang, S., Andersen, K. H., Lunne, T. & Yetginer, G. (2020). Effect of sample disturbance on cyclic shear strength of normally to lightly oc clays. *International Journal of Geotechnical Engineering* 14, No. 3, 242–253.

Zografou, D., Gourvenec, S. & O'Loughlin, C. (2019). Response of normally consolidated kaolin clay under irregular cyclic loading and comparison with predictions from the accumulation procedure. *Géotechnique* 69, No. 2, 106–121.

Accepted manuscript doi:
10.1680/jgeot.22.00010

Table 1. Summarize of test program.

Test	Description	w_i [%]	w_r [%]	gma_{a0}' [kPa]	K_0 [-]	τ_{av} [kPa]	G_{max} [MPa]	τ_{max}^{cy} [kPa]	soil sample consolidation
IRL_A20	Irregular loading with average shear stress	60.8	54.5	100	0.6	20	25.3	21.4	anisotropic
IDL_A20	Idealised loading history of IRL_A20	60.5	54.5	100	0.6	20	26.9	21.4	anisotropic
MS_A20	Mix-sorted IDL_A20	60.6	51.9	100	0.6	20	24.6	21.4	anisotropic
IDL_A0	Idealised loading without average shear component	57.7	47.7	150	1	0	37.5	40.2	isotropic
MS_A0	Mix-sorted IDL_A0	57.7	47.5	150	1	0	39.7	40.2	isotropic

In the table: w_i : initial water content; w_r : water content after consolidation; σ'_{a0} : effective axial consolidation stress; K_0 : earth coefficient at consolidation, $k_0 = \sigma'_{r0} / \sigma'_{a0}$; τ_{av} : target shear stress at consolidation; G_{max} : small strain shear modulus; τ_{max}^{cy} : target maximum cyclic shear stress

Table 2. Idealised load history IDL_A20 and IDL_A0.

Loading package	$\tau_{cy} / \tau_{max}^{cy}$	No. of cycles N
1	0.05	230
2	0.15	258
3	0.25	209
4	0.35	107
5	0.45	60
6	0.55	24
7	0.65	12
8	0.75	6
9	0.825	1
10	0.875	1
11	0.925	1
12	1	1
Reference cycles	1	until failure

Table 3. Mix-sorted idealised history MS_A20 and MS_A0

Loading parcel	$\tau_{cy} / \tau_{max}^{cy}$	No. of cycles N
1	0.25	4
2	0.55	6
3	0.25	25
4	0.65	6
5	1	1
6	0.65	2
7	0.925	1
8	0.65	4
9	0.35	107
10	0.25	49
11	0.05	50
12	0.55	12
13	0.45	30
14	0.15	100
15	0.55	6
16	0.75	6
17	0.05	100
18	0.25	100
19	0.45	15
20	0.825	1
21	0.45	15
22	0.875	1
23	0.25	31
24	0.15	158
25	0.05	70
Reference cycles	1	until failure

Figure captions

Figure 1. Definition of stress and strain components.(a) Stress components (b) strain components

Figure 2. Illustration of test programs (loading histories).(a)loading history IRL_A20(c)loading history MS_A20(d)loading history IDL_A0(e)loading history MS_A0

Figure 3. Experimental results of the 5 load histories. For each load case, the normalised stress path ($\tau / \sigma'_{a0} \sim \sigma'_a / \sigma'_{a0}$), the normalised stress-strain response ($\tau / \sigma'_{a0} \sim \gamma$) and the normalised stress-pore water pressure ratio ($\tau / \sigma'_{a0} \sim u_p / \sigma'_{a0}$) are given (from left to right).(a)load case IRL_A20 (b)load case IDL_A20 (c)load case MS_A20 (d)load case IDL_A0 (e)load case MS_A0

Figure 4. Shear strain γ versus time t for representative loading case IRL_A20, IDL_A20 and MS_A20. Load histories are presented as $\tau / \sigma'_{a0} \sim t$ (shear stress ratio sim time) for informative purpose.(a)Irregular loading history IRL_A20. (b)Idealised loading history IDL_A20. (c)Newly sorted idealised loading history MS_A20.

Figure 5. Strain evolution of the reference cycles applied after load histories IRL_A20, IDL_A20 and MS_A20.

Figure 6. Stress-strain behaviour of the first reference cycle applied after load histories IRL_A20, IDL_A20 and MS_A20.

Accepted manuscript doi:
10.1680/jgeot.22.00010

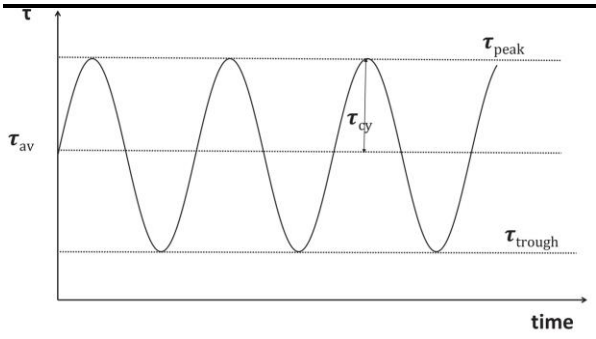

liufig01a

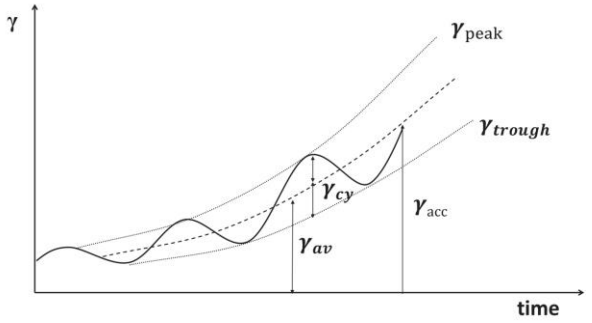

liufig01b

Accepted manuscript doi:
10.1680/jgeot.22.00010

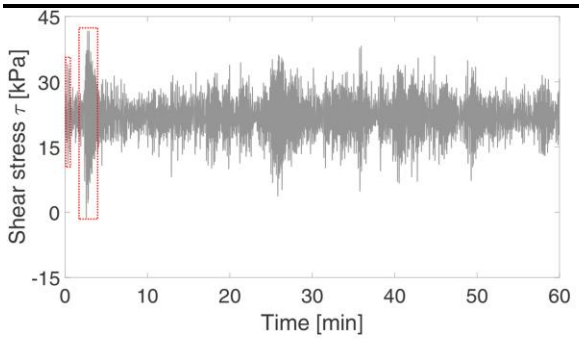

liufig02a

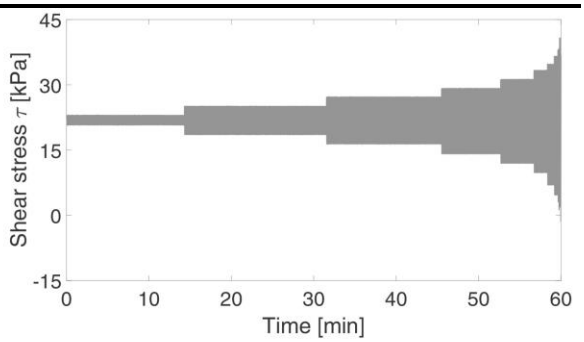

liufig02b

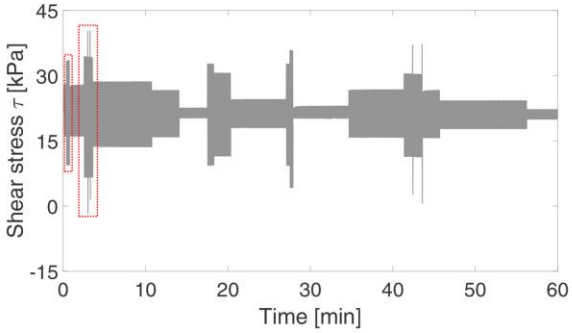

liufig02c

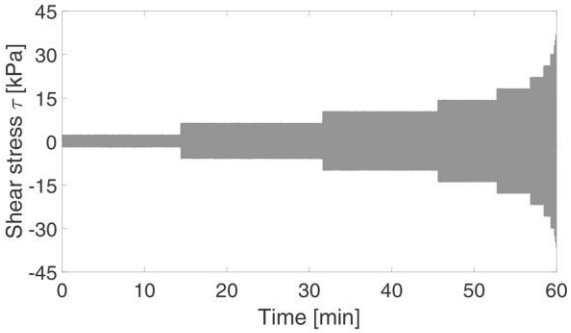

liufig02d

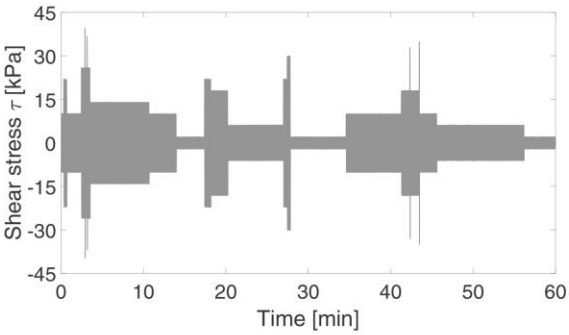

liufig02e

Accepted manuscript doi:
10.1680/jgeot.22.00010

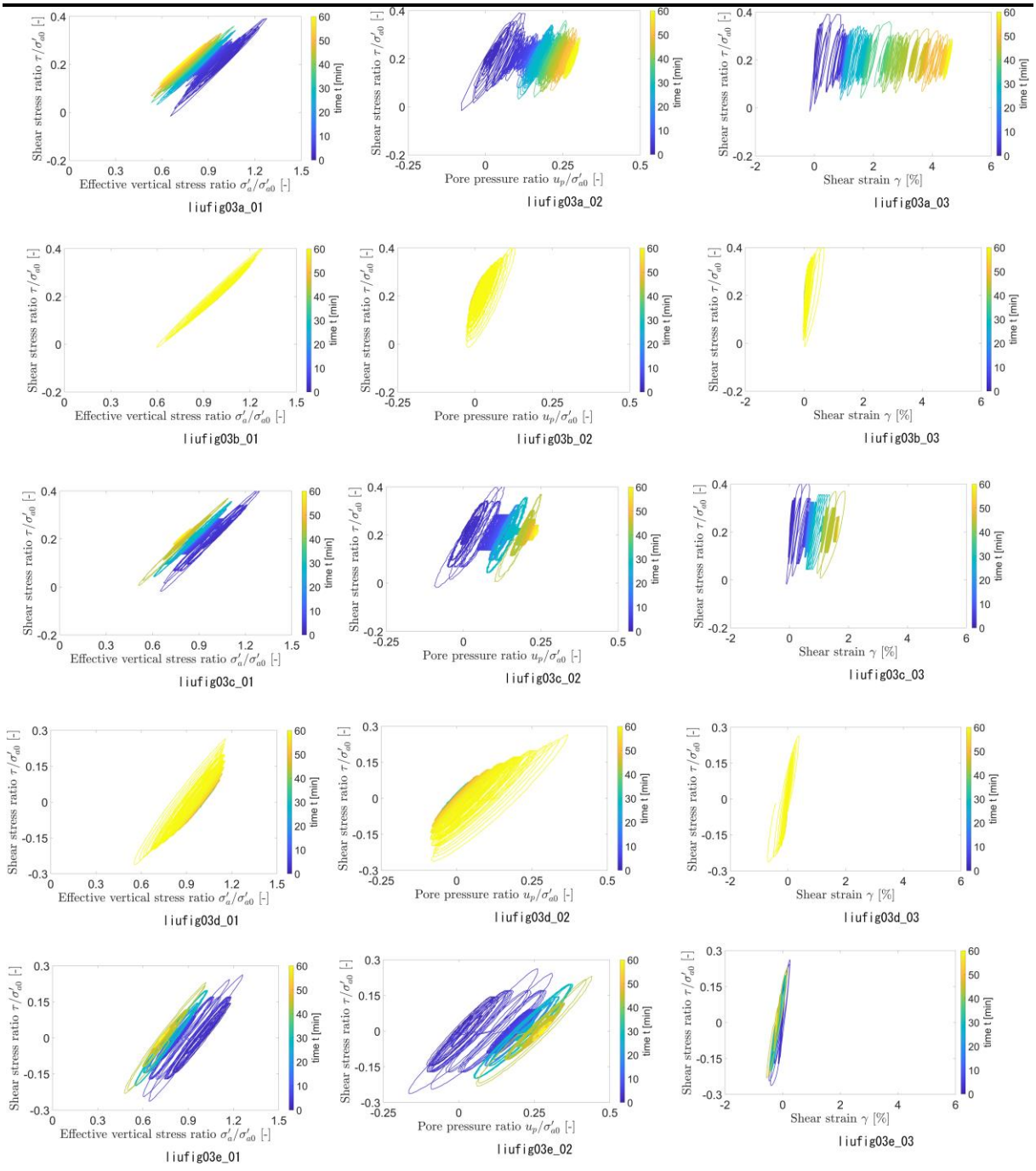

Accepted manuscript doi:
10.1680/jgeot.22.00010

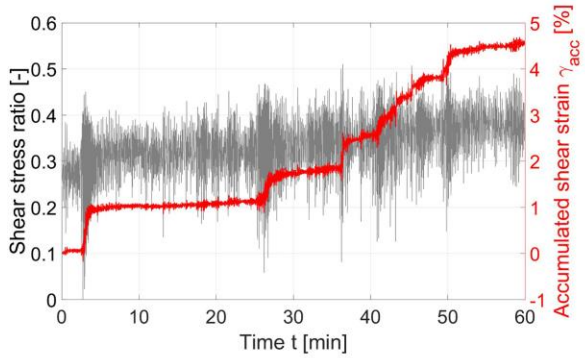

liufig04a

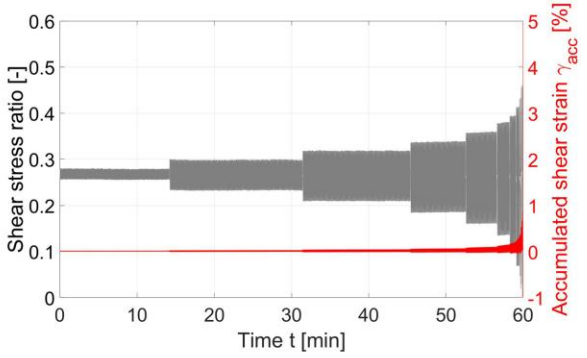

liufig04b

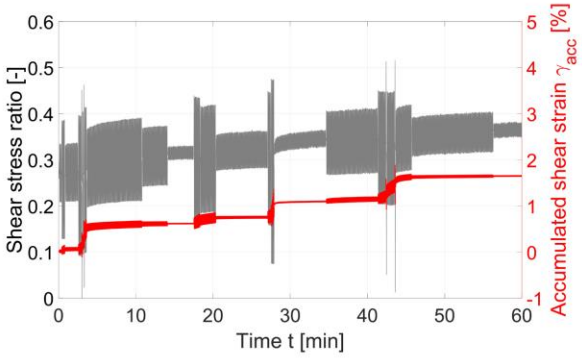

liufig04c

Accepted manuscript doi:
10.1680/jgeot.22.00010

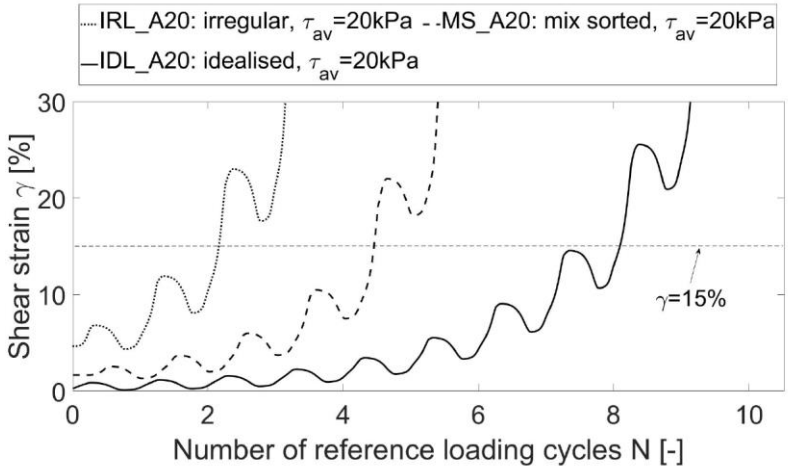

liufig05

Accepted manuscript doi:
10.1680/jgeot.22.00010

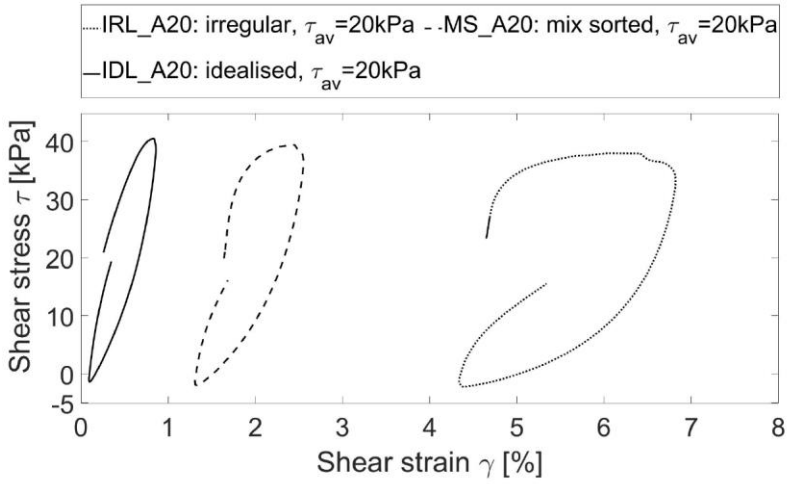

liufig06

Accepted manuscript doi:
10.1680/jgeot.22.00010

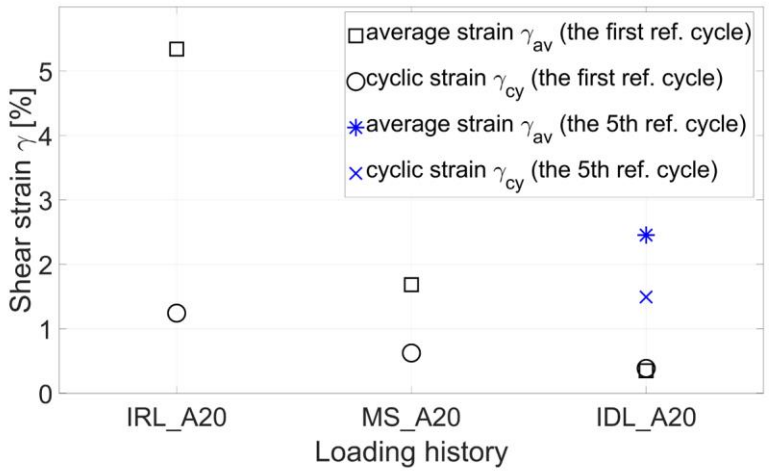

liufig07

Accepted manuscript doi:
10.1680/jgeot.22.00010

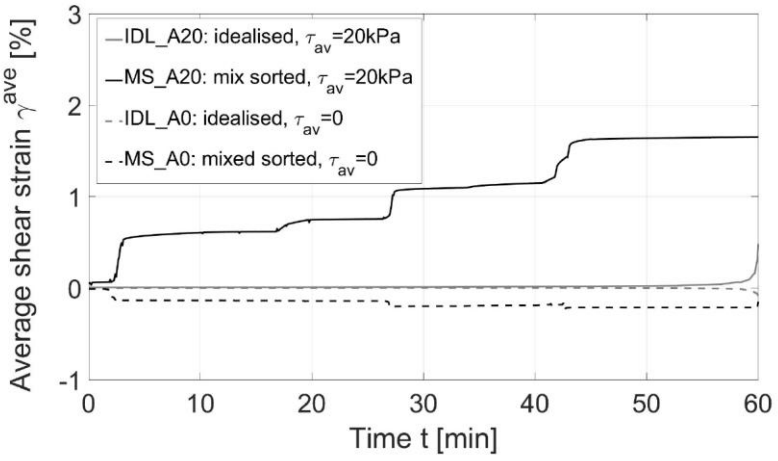

liufig08

Accepted manuscript doi:
10.1680/jgeot.22.00010

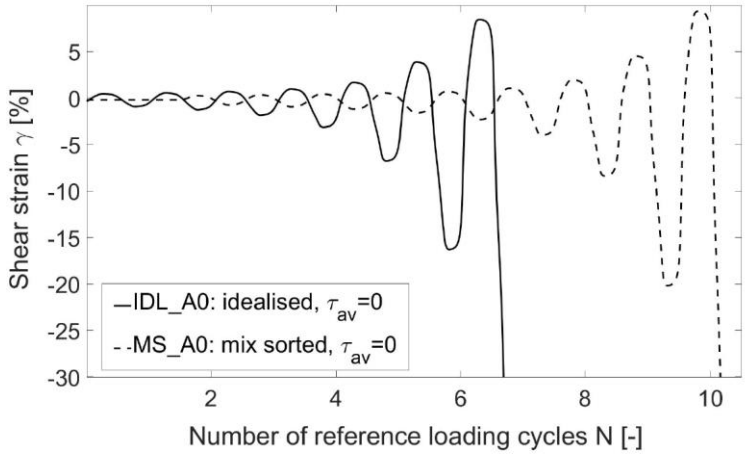

liufig09

Accepted manuscript doi:
10.1680/jgeot.22.00010

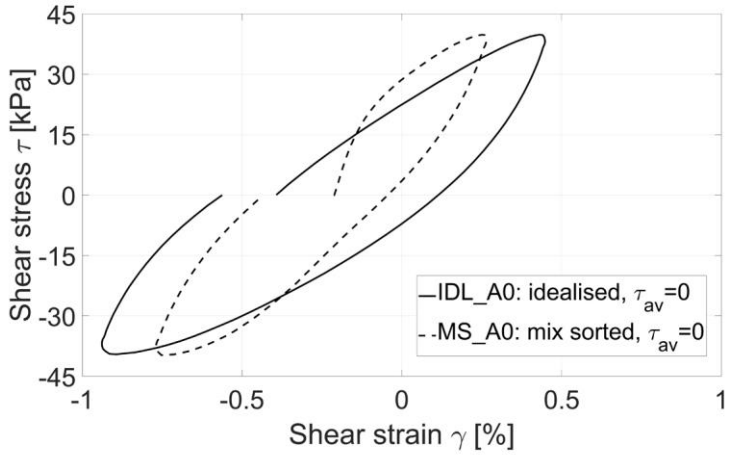

liufig10

Accepted manuscript doi:
10.1680/jgeot.22.00010

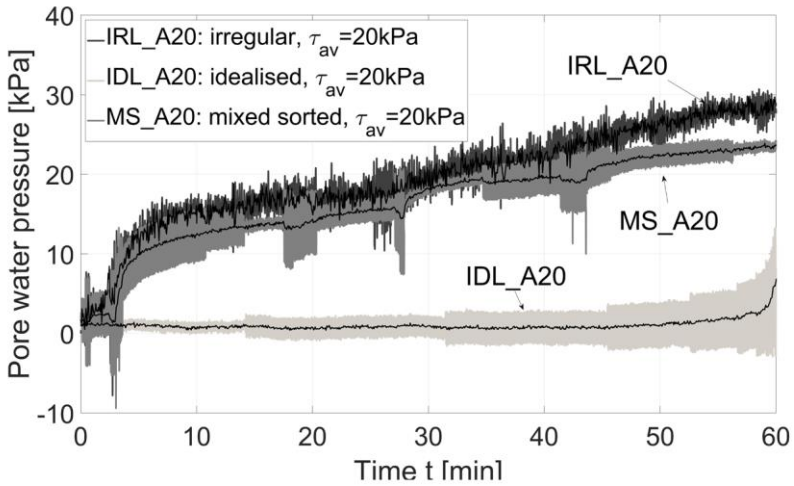

liufig11

Accepted manuscript doi:
10.1680/jgeot.22.00010

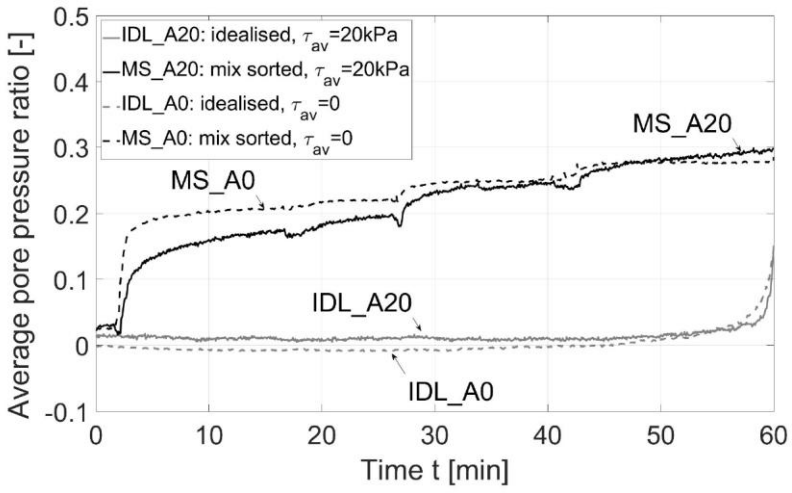

liufig12

Accepted manuscript doi:
10.1680/jgeot.22.00010

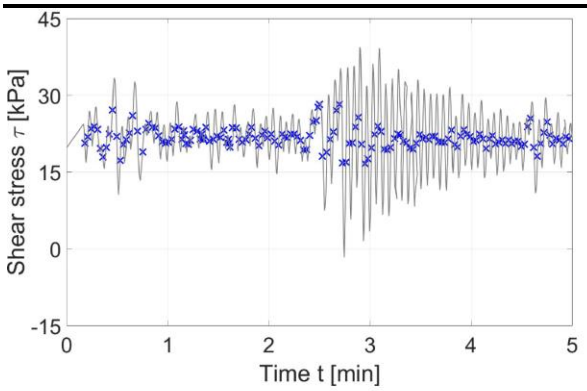

liufig13a

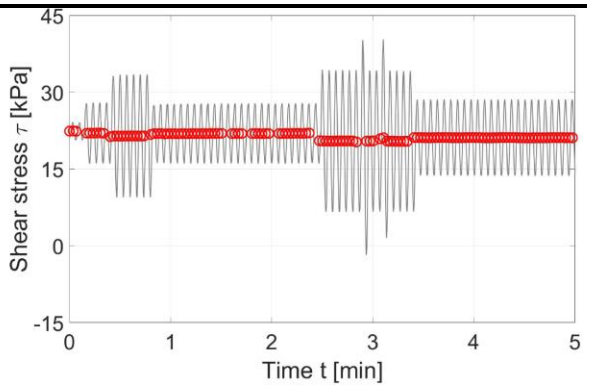

liufig13b

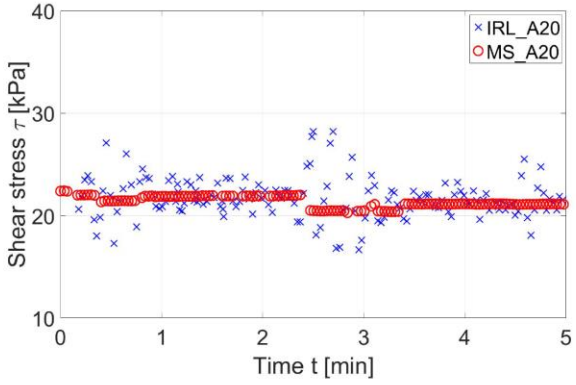

liufig13c